Surface Viscoelasticity Studies of Ultrathin Polymer Films Using Atomic Force Microscopic Adhesion Measurements

X. P. Wang, Xudong Xiao, and O. K. C. Tsui*

Physics Department, Hong Kong University of Science and Technology, Clear Water Bay, Kowloon, Hong Kong, China

Received November 2, 2000; Revised Manuscript Received February 5, 2001

ABSTRACT: Many applications of polymer thin films are determined by the molecular structure and chain mobility at the polymer-air surface. In ultrathin polymer films where the film thickness is comparable to the size of the macromolecule, chain connectivity, for example, may mediate effects of the substrate to the polymer-air surface, giving rise to suppression of the surface segmental mobility. In a previous study, we showed that atomic force microscopic adhesion measurements (AFMAM) could be used to quantify the dynamics in the upper ∼10 nm surface layer of polymer thin films near the glass-to-rubber transition. In this study, we use AFMAM to investigate the surface dynamics of ultrathin films of poly(*tert*-butyl acrylate) (P*t*BuA), to look for any systematic variation in the surface chain mobility as the film thickness, d is varied from $\sim 1\langle R_g \rangle$ to $13\langle R_g \rangle$. Suppression in the tip−sample adhesion was observed when d became < 20 nm ($\sim 2\langle R_g \rangle$), suggesting that the extent of the substrate effect is of the order of the size of a macromolecule in the present system.

Introduction

In a variety of polymer thin film applications, such as adhesion, lubrication, and liquid crystal display, the molecular structure and segmental mobility at the free surface or the polymer-air interface within a few segmental lengths dictates the functionality of the thin film. In ultrathin polymer films where the thickness is comparable to the radius of gyration, R_g, of the polymer molecule, many unusual dynamic properties have been found.[1−9] For example, the glass-to-rubber transition temperature, T_g, of polystyrene thin films of this thickness dimension were found to be depressed with respect to the bulk T_g by up to ∼20 °C when the thin films were deposited on silicon substrates covered with a layer of native oxide[1] but ∼70 °C when the thin films were free-standing.[2] The opposite behavior has also been observed, but in other polymer thin film systems.[3−5] With supported polymer films, the very fact that the polymer film does not dewet from the underlying substrate demonstrates that the polymer is adherent to the substrate or that the polymer-substrate interaction has to be attractive.[10] From this point of view, supported polymer thin film systems wherein the T_g decreases with decreasing film thickness necessitate the existence of a mechanism that opposes the attractive interaction at the polymer-substrate interface. It has been suggested that the molecular dynamics of the polymer is enhanced near the free surface[6,7] but suppressed near an attractive substrate.[4,5,8,9] Several experiments showed that such effects of the substrate exist and can be long-ranged.[4,5,8,9] For example, the thermal expansion of polystyrene thin films—a measure of the free volume of the polymer, which has been shown to be directly related to the segmental mobility both on an experimental basis and on the basis of physical arguments[11]—was found to be suppressed within $\sim 15R_g$ from the substrate wall.[4,5] This, together with the abundant experimental evidence for the thickness dependence of T_g found recently in many supported polymer ultrathin film systems, suggests that a characteristic length of the order of R_g may exist over which the dynamics of the segments are perturbed by the substrate. In this paper, we elucidate the use of AFMAM to probe this effect of the substrate. Previously, we showed that AFMAM could be used to characterize the surface viscoelasticity of P*t*BuA (M_w = 148 kDa, M_w/M_n = 17) near the T_g of the sample.[12] In this study, we vary the thickness of thin films of this polymer from 10 to 133 nm ($\sim 1-13\langle R_g \rangle$), for the purpose of adjusting the long-range effects of the substrate if they exist in this polymer thin film system.

Experimental Section

Sample Preparation. The sample P*t*BuA (T_g = 50 °C by DSC) was purchased from Scientific Polymer Products, New York. The substrates are silicon (100) single crystals with surface roughness less than 1 nm. To clean the substrates, the Si wafers are first dipped into a mixture of H_2SO_4 and H_2O_2 (in 10:1 volume ratio) at 120 °C for 10 min., followed by thorough rinsing in deionized water. They are then dipped into a mixture of HF and H_2O (in 1:50 volume ratio) for 1 min, followed by thorough rinsing in deionized water before they will be blown dry in N_2 gas. Between one to a few days after the substrates are cleaned, ellipsometry reveals that a native oxide overlayer that is ∼1.5 nm thick will form, whereupon the substrates will be used to make the samples. The thin film samples were prepared by spin coating solutions of P*t*BuA in toluene (0.3−2 wt %) onto the cleaned silicon substrates. Film thicknesses were measured by variable-angle spectroscopic ellipsometry. Before the initial study, all samples were annealed under 10^{-3} Torr vacuum at 120 °C overnight to relax the polymer and to remove any residue solvent.

AFM Adhesion Measurements. AFM experiments were performed in a home-built AFM controlled by RHK electronics (RHK Technology). Temperature was controlled between room temperature and 80 °C to within ±1 °C stability by adjusting the dc current running through a Peltier heater. Commercial V-shaped silicon nitride integrated tip/cantilevers (Parks Scientific Instruments) with a nominal force constant, $k_c \sim 0.5$ N m^{-1}, and the radius of the tip apex, $R \sim 50$ nm, were used. The whole setup was kept inside a glovebox where the humidity was controlled to < 10%, at which water capillary

* To whom correspondence should be addressed. E-mail: phtsui@ust.hk.

10.1021/ma0018953 CCC: $20.00
Published on Web 05/05/2001

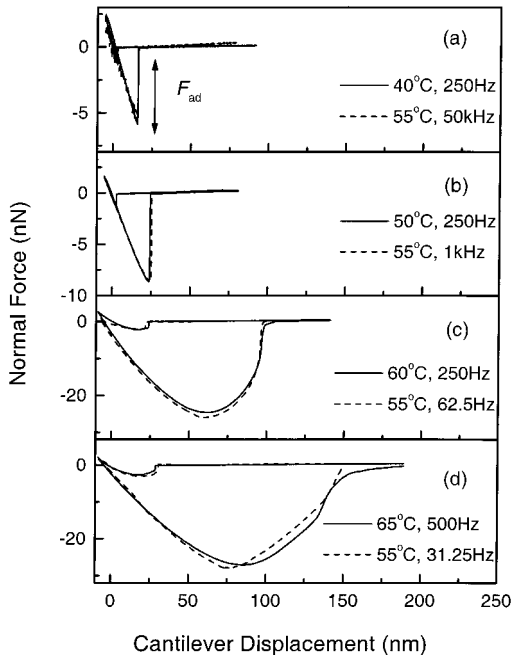

Figure 1. (a−d) Typical $F-D$ curves obtained from the P*t*BuA thin films at four different pairs of equivalent $T-f$ conditions (see text) near the T_g.

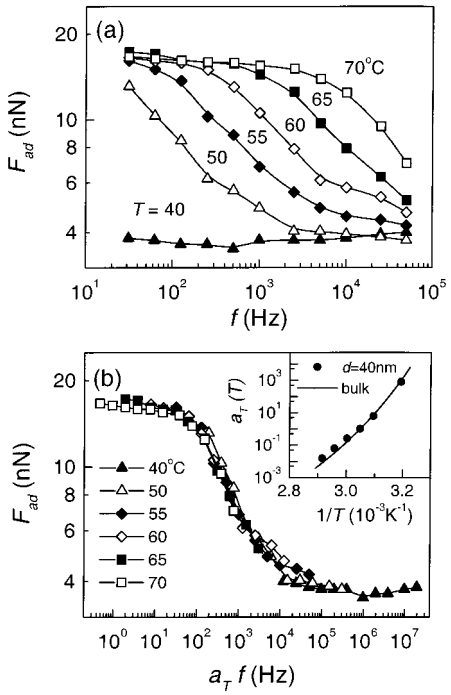

Figure 2. (a) F_{ad} obtained for a $d = 40$ nm sample at $F = 2.5$ nN as a function of f at various T as labeled. (b) (main panel) Master curve $F_{ad}(a_T(T)f)$ obtained from data depicted in part a with $T_{ref} = 55$ °C. Here, solid lines are guides-to-the-eye. (inset) Arrhenius plot for the shift factors used to produce the master curve in the main panel (solid circles). The solid line is data of the bulk.

force is negligible. To produce tip advancement (withdrawal), incremental (decremental) voltage steps of adjustable duration δt are applied to the piezoelectric actuator that controls the cantilever displacement. We define the probe rate, $f = 1/\delta t$, which can be viewed as the rate at which loading and unloading forces were exerted onto the sample. The loading force, defined as the force applied to the tip whereat tip advancement terminates, is controlled to ∼2.5 nN. For more details of the experimental setup and procedure, the readers are referred to an earlier paper published by us.[12] Parts a−d of Figure 1 show a representative set of approach−retract force−distance ($F-D$) curves obtained at various stages near the glass-to-rubber transition of the sample. In these figures, the vertical axis is the normal force experienced by the cantilever due to interactions between the tip and the sample. The horizontal axis is the displacement of the cantilever produced by the piezoelectric actuator to which the cantilever is attached. Adhesion, F_{ad} was generally determined from the $F-D$ curves as the pull-off force with which detachment between the tip and the sample occurred (Figure 1, parts a and b). However, when the polymer was soft, the $F-D$ curves display a prominent curvature (Figure 1, parts c and d), and no abrupt, distinctive interfacial breakage of the sample/tip adhesive bond could be seen. Adhesion was then determined as the maximum pull-off force noted in the $F-D$ curve. As pointed out in ref 12, development of curvature in the $F-D$ curve indicates that the effective force constant of the sample, k_s (which equals the force exerted onto the sample via the tip divided by the resulting sample deformation, δ, is a function of the sample elastic modulus and the instantaneous sample/tip contact area), is becoming comparable to that of the cantilever, k_c, as the sample/tip contact area diminished during tip pull-off. By the balance of force between the tip and the sample, i.e., $k_s\delta = -k_c\delta_{tip}$ (where δ_{tip} is the amount of bending in the cantilever), it follows that upon onset of curvature in the $F-D$ curves, the sample should assume deformations comparable to the deformation undertaken by the cantilever. Existence of an extended deformation tail (>∼50 nm) following development of curvatures in an $F-D$ curve as seen in Figure 1, parts c and d, therefore, evidences plastic deformation in the sample. Failure in the sample/tip bonding most likely occurred through cohesive fracture. Physically, adhesion is defined for cases as such is essentially the "effective yield strength" of the polymer pulled out at unloading; i.e., it is the force at which the amount of increase in the stress within the sample/tip system due to an extension in the polymer exactly cancels with the amount of decrease in the stress due to the resultant reduction in the effective force constant of the polymer/tip contact. The round-bottomed feature associated with such yield in the sample/tip contact (Figure 1, parts c and d) will show in the $F-D$ curve only if it precedes the (sharp) interfacial sample/tip detachment. As the polymer softens, the effective yield strength lowers naturally with the elastic modulus while the interfacial adhesive bond strength increases (for which the explanation will be postponed until a later section). This lowering in the effective sample yield strength and rise in the interfacial adhesive bond strength upon softening of the polymer consequences the former to become smaller than the latter at sufficiently high temperatures or low probe rates, resulting in occurrence of the round-bottomed feature in the $F-D$ curve found in Figure 1, parts c and d.

Results

Figure 2a shows F_{ad} vs f obtained for a 40 nm thick film at a loading force, $F = 2.5$ nN, at different temperatures, T near the T_g. Experimentally, F is controlled by bringing the tip into bending by a fixed amount equals 5 nm. A loading force of 2.5 nN is thus determined by assuming the nominal value of 0.5 N m^{-1} for the force constant of the cantilever. As seen, at any given T, $F_{ad}(f)$ showed a rise followed by saturation as f was decreased. In the low-f region where F_{ad} saturated, the $F-D$ curve displayed a distinctive tail that extends more than the thickness of the film. According to the discussion in the previous section, the sample/tip bond fracture is most likely cohesive in this frequency range. With T increased, the same shape was found for $F_{ad}(f)$ but the onset frequency shifted to a higher value. This is characteristic of any dynamic function near the glass-to-rubber transition.[13] For polymers, this dynamic behavior has been identified with the main chain or

Table 1. Results Obtained from Least-Squares Fitting of the $a_T(T)$ Data in Figure 4 to the VTF Relation in Eq 1

	d (nm)							
	15	20	40	62	80	98	133	bulk
B (K)	1161 ± 250	999 ± 31	953 ± 133	990 ± 51	836 ± 119	1000 ± 10	999 ± 21	1063 ± 3
T_0 (K)	235 ± 10	244 ± 2	246 ± 6	243 ± 2	250 ± 5	242.4 ± 0.5	244 ± 1	242.6 ± 0.1

segmental motion.[11] We rescaled the abscissa of each curve with a temperature-dependent shift factor, $a_T(T)$ using 55 °C as the reference temperature, T_{ref} (i.e., We define $a_T(55\ °C) \equiv 1$). The curves overlap into a master curve, $F_{ad}(a_T f)$ as shown in the main panel of Figure 2b. This time−temperature equivalence property of the dynamics can also be observed in the $F-D$ curves. As demonstrated in Figure 1, parts a−d, the four pairs of $F-D$ curves (solid and dashed lines) that are obtained at four different pairs of equivalent $T-f$ conditions are the same. ((T_1, f_1) and (T_2, f_2) are equivalent if $f_2 = [a_T(T_1)/a_T(T_2)]\, f_1$.) The inset of Figure 2b shows the Arrhenius plot for the shift factors (solid circles) that had been used to produce the master curve in the main panel. The solid line shows the shift factors of a bulk sample deduced from torsion and shear modulus measurements.[12] Assuming the typical Vogel−Tamman−Fulcher (VTF) relation[14] for the relaxation time, $\tau(T)$ ($\equiv 1/f(T)$), we have

$$a_T(T) = a_T(T_{ref}) e^{B/(T-T_0)-B/(T_{ref}-T_0)} \qquad (1)$$

where T_0 is the Tammann temperature, ~50 K below the T_g, and B is a constant related to the fragility of the polymer (where the more fragile the glass-former is, the smaller the value of B will be). Physical meaning of T_0 and fragility had been proposed by Angell[15] on the basis of Adam and Gibbs's theory of glass transition.[16] According to Angell, T_0 was identifiable with the Kauzmann temperature, T_K, at which the configurational entropy of a supercooling liquid vanishes.[17] This identification provides a physical explanation for the divergence of $\tau(T)$ at T_0 that eq 1 implies. On the other hand, fragility reveals the density of local minima in the potential energy hypersurface governing the dynamics relevant to the glass-to-rubber transition. Therefore, the more fragility the glass is, the more readily the configurational entropy of the glass will be frozen in as temperature is lowered near the T_g. If the segmental mobility of the polymer at the free surface is enhanced with respect to the bulk, one would expect values of T_0 or B to be smaller for the data acquired with the AFM. By fitting the data of $a_T(T)$ in Figure 2b to eq 1, we obtain $B = 1063 \pm 3$ and 953 ± 133 K and $T_0 = 242.6 \pm 0.1$ and 246 ± 6 K for, respectively, the bulk and the 40 nm thick film. Good agreement between the two sets of fitted results evidences against the segmental mobility at the free surface of a $d = 40$ nm P*t*BuA thin film being higher than that in the bulk. However, we postpone making any conclusion until we have compared data of the other thicknesses.

Figure 3 shows the adhesion master curves for all the P*t*BuA thin films studied ($d = 10-133$ nm) with the same load of ~2.5 nN. For each curve, the vertical axis is the measured adhesion normalized by the asymptotic value at high frequencies, $F_{ad}(a_T f)/F_{ad}(\infty)$ and the horizontal axis is the rescaled frequency, $a_T(T)f$. Arrhenius plots for the shift factors $a_T(T)$ used to produce the master curves (symbols), together with the data obtained by torsion and shear modulus measurements of the bulk sample (solid line) are shown in Figure 4. We

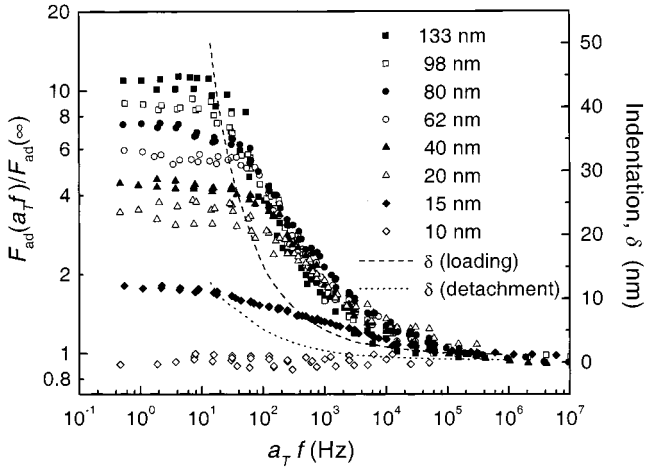

Figure 3. Adhesion master curves obtained for films of different d at a load of 2.5 nN. The dashed line is the indentation of the sample by the tip at the loading force estimated by the JKR model. The dotted line is the sample indentation at detachment, also estimated by the JKR model.

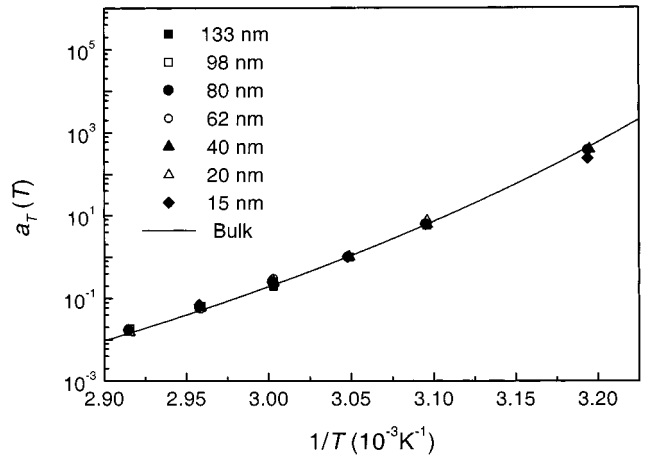

Figure 4. Arrhenius plots for the $a_T(T)$ used to produce the master curves shown in Figure 3. The solid line is data of the bulk.

model fit data of Figure 4 by eq 1 and tabulate the results in Table 1. As seen, the fitted values of both parameters B and T_0 agree quite well among one another, with no obvious dependence on the film thickness, d. On the basis of these fitted results, we conclude that the segmental mobility, least of the dynamically active modes, at the free surface of P*t*BuA is not affected by the change in the degree of proximity to the substrate.

On the other hand, the mechanical property of the P*t*BuA thin films does not likewise show independence with d. As seen in Figure 3, the shape of the adhesion master curves of $d = 10$ and 15 nm deviate substantially from those of the other films. For the thin films with $d \geq 20$ nm, the shape of the adhesion master curve is more or less independent of the film thickness in the high-frequency regime until saturation in adhesion commences at lower frequencies, where as we have argued above, the sample/tip bond fracture occurs cohesively.

Previously, we devised a mechanical analysis for the interpretation of the rate-dependent adhesion data, $F_{ad}(f)$,[12] which shows that $F_{ad}(f) \sim 1/E(1/f)$ as long as interfacial adhesive bond fracture prevails. We will outline the calculation below.

Discussions

It has been found that the stress distribution, $\sigma(r)$ at the contact between a linearly elastic sphere and a flat surface is[18]

$$\sigma(r) = \frac{2E}{\pi R(1-\nu^2)}\sqrt{(a^2 - r^2)} - \sqrt{\frac{2E\gamma a}{\pi(1-\nu^2)(a^2 - r^2)}} \quad (2)$$

where r is the distance measured from the center of the contact, a the contact radius between the polymer and the tip, γ the interfacial energy between the two adhering objects, ν the Poisson ratio and E the Young's modulus of the polymer. On the right-hand side of eq 2, the first term comes from the compressive pressure in the central region and is associated with the center of mass motion of the adhering objects. The second term comes from the tensile stress at the periphery of the contacting area and governs the propagation of the crack tip during adhesive bond fracture. To extend the validity of eq 2 to viscoelastic cases as in the present one, one may replace the elastic modulus, E in the equation by the time-dependent elastic modulus, $E(t)$ of the viscoelastic solids.[18] However, we note that the time scales involved in the propagation of a crack tip are much shorter than those of the center of mass motion.[12] Furthermore, for the probe rates employed in this experiment ($f = 31.25-50$ kHz), the time scale of the center of mass motion falls in the range where $E(f)$ varies notably (according to dynamic measurements of the bulk[12]). Therefore, we replace E in the first term on the right-hand side of eq 2 by $E(t)$ but that in the second term by the instantaneous elastic modulus, $E(0)$. The stress distribution pertaining to our experimental conditions should therefore be modified to

$$\sigma(r) = \frac{2E(t)}{\pi R(1-\nu^2)}\sqrt{(a^2 - r^2)} - \sqrt{\frac{2E(0)\gamma a}{\pi(1-\nu^2)(a^2 - r^2)}} \quad (3)$$

By writing $E(0)\gamma = E(t)\gamma_{eff}$, eq 3 recovers the same form as eq 2 but with a different surface energy $= \gamma_{eff} = E(0)\gamma/E(t)$. By using the result from the JKR model[19] for linearly elastic solids, namely $F_{ad} = 3\pi\gamma R/2$, one may deduce that the time-dependent adhesion of viscoelastic solids, $F_{ad}(t)$, should modify to

$$F_{ad}(t) = 3\pi\gamma R E(0)/2E(t) \quad (4)$$

In Figure 5 is plotted $E(0)/E(t)$ (solid line), where $E(t)$ was the Fourier transformation of the dynamic elastic modulus of the bulk sample determined from shear and torsion measurements. In the same graph is also plotted the normalized adhesion, $F_{ad}(t)/F_{ad}(0)$ (solid line) as a function of t ($\equiv 1/f$) (solid circles) for a 133 nm thick P*t*BuA film. The two sets of data agree with one another quite well. Deviations observed in longer times $t \geq 50$ ms can be understood as due to changes in the nature of the adhesive bond fracture from being interfacial to cohesive as discussed before.

On the basis of the above result, we will interpret the adhesion master curves shown in Figure 3 for P*t*BuA ultrathin films of different d. The calculation simply illustrates that $F_{ad}(t) \sim 1/E(t)$, where $E(t)$ is the time-dependent elastic modulus of the polymer in the proximity of the contact region between the tip and the sample. The fact that the shape of the adhesion master curves found for all films thicker than 20 nm is independent of the film thickness (Figure 3) and that it coincides with $1/E(t)$ of the bulk at high frequencies before the plateau region is reached (as Figure 5 illustrates) suggests that the mechanical strength of the polymer at the free surface is the same as the bulk, and is not affected by the presence of the substrate that is as near as ~20 nm. These results are in keeping with the above findings that no difference in the shift factor data is detected between those obtained by the AFM and those obtained by bulk torsion and shear modulus measurements. It may be argued that the presence of an AFM tip in contact with the surface of a polymer may alter the local mechanical property of the polymer by, for example, changing the equilibrium population of the chain ends. However, modifications of this kind involve structural rearrangements of the polymer segments, hence should require times on the order of hours.[20] Since the measurement times of this experiment are less than a second, we do not think that such effect will be effective in our study.

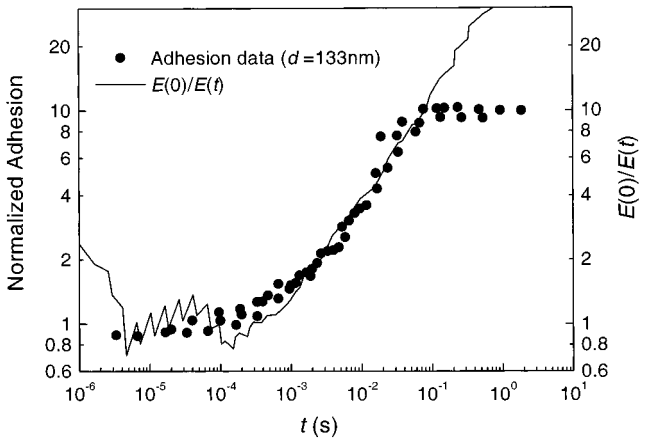

Figure 5. Comparison between data for $F_{ad}(t)/F_{ad}(0)$ of a 133 nm thick sample taken at $F = 2.5$ nN (solid circles) with $E(0)/E(t)$ (solid line). Oscillations in the $E(t)$ data are artifacts that come from the Fourier transformation process.

Following the foregoing interpretation that the surface segmental mobility of P*t*BuA films for $d = 20-133$ nm is independent of d, and is the same as the bulk, it is not immediately obvious why there are deviations in the adhesion curves observed in the plateau region among different d (Figure 3). In the plateau region, the polymer suffers mechanical yield and the sample/tip bond fracture occurs cohesively, which invalidates the viscoelasticity model described above. In this mechanical regime, the radius of the sample/tip contact area, a, (and hence the indentation of the tip into the sample, $\delta = R - \sqrt{(R^2 - a^2)}$) at the loading force of 2.5 nN becomes an important parameter to consider as it is directly related to the size of the cohesively fracturing weak link in the polymer that is being pulled out. Indentation of the tip into the sample, which is a function of the sample elastic modulus, sample/tip adhesion and applied load, can be estimated using the JKR model.[19] The tip indentation at loading as a function of f has been calculated for this experiment and is shown in Figure 3 by the dashed line. As seen, δ remains $\leq 10-15$ nm for most part of the frequency range studied. But near the low-frequency regime where the adhesion master curves saturate, δ

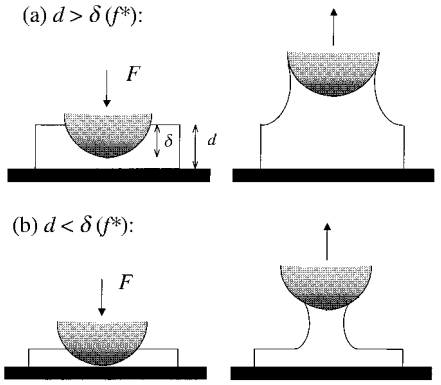

Figure 6. Schematic diagram illustrating how the polymer film thickness may affect the cohesive bond strength in the low-frequency region by limiting the size of the cohesively fracturing weak link that can form in the polymer.

rises and reaches 50 nm rapidly as f decreases. When δ is greater than 50 nm (∼radius of the tip apex, R), the JKR model, which has been constructed for a spherical indenter, will become inapplicable. However, it is reasonable to assume that δ continues to grow beyond this point with decreasing f as the polymer continues to soften. It should, however, be understood that this calculated result of $\delta(f)$ only provides a crude estimate since it was $E(t)$ of the bulk (rather than the $E(t)$ of the polymer at the free surface which is still an unknown to be determined) and the nominal value of the cantilever force constant ∼ 0.5 N m^{-1} (which may deviate substantially from the actual value[21]) that had been used in the calculation. Therefore, the simulated result of δ depicted in Figure 3 should be regarded as a guideline for the qualitative behavior only. Imagine that at a sufficiently low frequency, f^*, e.g., $\delta(f^*)$ becomes equal to the film thickness, d. From this point on, for any $f \leq f^*$, the tip indentation will always be d at loading since further tip advancement will be stopped by the substrate at the bottom. This will lead to a thickness dependence of the sample/tip contact radius at loading, and hence a thickness dependence of the cohesively fracturing weak link in the polymer in the low-frequency regime as Figure 6 illustrates. This picture offers a qualitative explanation for the distribution of (cohesive) adhesion bond strength, which gets bigger for thicker films, in the plateau region Figure 3 displays. The observation that the onset frequency of the plateau region, which should just be $f^*(d)$ unless if cohesive bond fracture has not yet commenced, is smaller for thicker films also fits well into this interpretation. Because δ is a function of the loading force, F, the onset frequency of the plateau region should change if cantilevers of different stiffness are used. A variation in the onset frequency was indeed found for P*t*BuA thin films with similar thicknesses[22] when AFM cantilevers from different batches were used for the experiment. Therefore, quantitative analysis of the adhesion data in the low-frequency region will necessitate a careful calibration of the cantilever force constant, k_c. In the present investigation, however, we only focus on the analysis in the high-frequency regime where eqs 3 and 4—the model for the *interfacial* adhesive force between a spherical indenter and a viscoelastic solid—is valid. In this regime, adhesion is independent of the loading force as eq 4 evidences. Therefore, k_c is not a critical parameter of the analysis. Inasmuch as only the high-frequency region is considered, the use of adhesion, F_{ad} (=the maximum pull off force noted in the $F-D$ curve) is entirely compatible with the use of the work of adhesion, W (=area under the $F-D$ curve) for the characterization of the adhesive bond fracture. This is because the $F-D$ curve is linear in this mechanical limit so that F_{ad} is proportional to W. In cases where the bond fracture occurs cohesively, however, the work of adhesion may be physical more meaningful.[23]

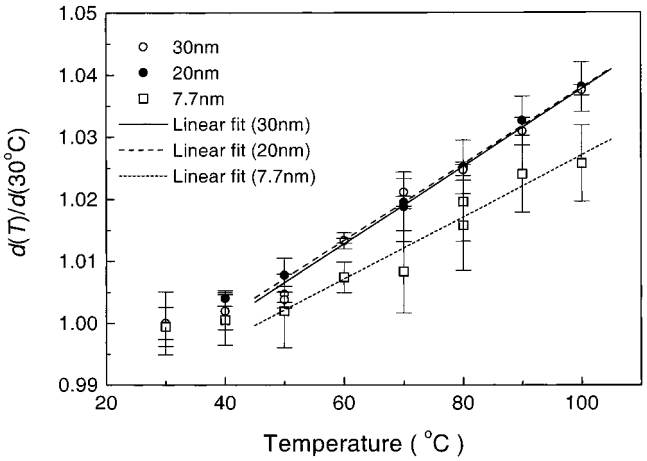

Figure 7. Plots of film thickness normalized by the value at 30 °C as a function of temperature for P*t*BuA films with d = 30, 20, and 7.7 nm.

We will now turn our attention to data of the 10 and 15 nm thick films. As seen in Figure 3, there is significant influence of the substrate on the measured adhesion. Using $F_{ad}(f) \sim 1/E(1/f)$, the data of Figure 3 suggest that the polymer film stiffens as the film thickness is reduced for d < 20 nm. On the other hand, no change can be detected in the corresponding shift factors in Figure 4. One possible interpretation is that a fraction of the polymer chains next to the substrate are immobilized to the extent where their dynamic activity is completely quenched over the dynamic range investigated in the present experiment. Since no lateral variation in F_{ad} was notable from measurements taken at more than 30 randomly sampled cites on the surface of the film, we believe that dynamic heterogeneity in our samples occurs along the normal direction of the film, which is consistent with what was proposed earlier that there might exist a dynamic dead layer immediate to the substrate wall.[4,5,24] NMR experiments of Blum et al.[25] on surface-bound poly(vinyl acetate) at monolayer coverage indeed discovered motional heterogeneity in the sample, with a component that remain immobile even at temperatures above the bulk T_g and another one that is more mobile than the bulk. We have measured the thermal expansion of P*t*BuA thin films with thicknesses equal 7.7, 20, and 30 nm by X-ray reflectivity. Shown in Figure 7 are the data plotted as film thickness normalized by the value at 30 °C as a function of temperature, T. Linear fits to the data above $T \geq 50$ °C, i.e., the bulk T_g, yields (4.98 ± 0.45), (6.15 ± 0.11), and (6.24 ± 0.28) × 10^{-4} °C^{-1} for the thermal expansion coefficients in the rubbery state, β_r, of, respectively, the 7.7, 20, and 30 nm thick films. The 22% suppression in β_r found in the 7.7 nm thick film, is similar to findings of refs 4 and 5 for other polymer thin film systems; are suggestive of an immobile dead layer in the polymer immediate to the substrate. However, we cannot exclude the possibility that the observations found in the d = 15 nm and especially the 10 nm thick films are due to the measurement technique itself. It is noteworthy that solutions to the JKR model or the modified one derived here (eq 4) are solutions[19] to the equilibrium states of the contact mechanical problem

involved in the AFMAM experiment. In other words, the derived solution at any particular stage of the contact process is due to the minimization of the total energy of the system, so it should have no bearing on how the contact has been made. From this point of view, it is more appropriate to look at the indentation at detachment to consider effects of the substrate on adhesion since adhesion is the force at detachment. (The use of indentation at loading in the earlier discussion for the consideration of adhesive bond strength in the plateau region of $F_{ad}(f)$ belongs to a different mechanical regime where the bond fracture occurs cohesively at a constriction in the polymer.) Indentation at detachment has been estimated for this experiment by the JKR model and is shown by the dotted line in Figure 3. As seen, adhesion of the $d = 15$ nm sample deviate substantially from the $1/E(1/f)$ behavior even for detachment indentations that are less than 2.5 nm. Within a value of indentation that is much smaller than d, it is difficult to imagine that the substrate may influence the interfacial bond fracture mechanically. On the other hand, if a dynamic dead layer indeed exists, the apparent thickness of the polymer will be reduced so that mechanical properties of the film detected by AFMAM will exhibit influence of the hard substrate at a larger than expected nominal film thickness. However, it is agreeable that a much more reliable check will be one that compares AFMAM data of ultrathin films of the same polymer, but deposited on different surfaces, with well-known interfacial interactions with the polymer. Studies are currently on going to clarify this important point. Finally, we remark that long-range van der Waals interaction between the substrate and the tip should be negligible in AFMAM. First of all, it is expected to add no more than ~50 Pa to the stress over the range of film thicknesses studied.[10] Second, adhesion of the $d = 15$ nm ultrathin film, being smaller than that of the thicker films, provides the strongest evidence against the suggestion that long-range van der Waals interaction between the tip and the substrate (which should fall off according to one over the distance squared) is at work.

Conclusion

In conclusion, we have reported in detail the use of AFMAM to study the dynamics of ultrathin films of P*t*BuA ($d \sim 1-13\langle R_g \rangle$) and the physical interpretations for the data were proposed. Adhesion master curves $F_{ad}(a_T f)$ were obtained with shift factors demonstrating no dependence on the film thickness. On the other hand, the shape of $F_{ad}(a_T f)$ (up to the point where mechanical yield in the polymer occurs) was found to be independent of d only for $d > 15$ nm. For $d \leq 15$ nm, suppression in $F_{ad}(a_T f)$ was found that elevates as d decreases. On the basis of the mechanical model proposed, we conclude that no difference in the dynamic behavior is detectable between the bulk and the free surface of P*t*BuA ultrathin films for $d > 15$ nm. However, for the $d \leq 15$ nm samples, the results are suggestive of an immobile component in the layer of polymer next to the substrate wall. This interpretation is consistent with results of independent thermal expansion coefficient measurements, in which a 22% reduction in the rubber thermal expansion was found in a 7.7 nm thick P*t*BuA film compared to values found for the 20 and 30 nm thick samples. If this picture of the $d \leq 15$ nm samples is correct, our result suggests that long-range effects from the substrate that influence the surface segmental mobility exist in the present polymer thin film system and they extend up to a distance of ~ 15 nm. As is expected from the fact that the polymer is adherent to the substrate, these effects tend to immobilize the polymer.

Acknowledgment. We acknowledge financial support of Hong Kong University of Science and Technology through the Research Grant Council of Hong Kong (RGCHK) under project no. DAG98/99.SC24. (O.K.C.T.), William Mong Solid State Clusters Laboratory and the High Impact Area Fund (X.P.W. and X.X.), as well as the RGCHK under Grant No. HKUST6139/97P (X.P.W. and X.X.).

References and Notes

(1) Keddie, J. L.; Jones, R. A. L.; Cory, R. A. *Faraday Discuss.* **1994**, *98*, 219.

(2) Forrest, J. A.; Kalnoki-Veress, K.; Stevens, J. R.; Dutcher, J. R. *Phys. Rev. Lett.* **1996**, *77*, 2002.

(3) Keddie, J. L.; Jones, R. A. L.; Cory, R. A. *Europhys. Lett.* **1994**, *27*, 59.

(4) Wallace, W. E.; van Zanten, J. H.; Wu, W. L. *Phys. Rev. E* **1995**, *52*, 3329.

(5) van Zanten, J. H.; Wallace, W. E.; Wu, W. *Phys. Rev. E* **1996**, *53*, R2053.

(6) Tanaka, K.; Takahara, A.; Kajiyama, T. *Macromolecules* **1997**, *30*, 6626.

(7) Hammerschmidt, J. A.; Gladfelter, W. L.; Haugstad, G. *Macromolecules* **1999**, *32*, 3360.

(8) Zheng, X.; Rafailovich, M. H.; Sokolov, J.; Strzhemechny, Y.; Schwarz, S. A.; Sauer, B. B.; Rubinstein, M. *Phys. Rev. Lett.* **1997**, *79*, 241.

(9) Lin, E. K.; Kolb, R.; Satija, S. K.; Wu, W. *Macromolecules* **1999**, *32*, 3753.

(10) Reiter, G.; Sharma, A.; Casoli, A.; Marie-Odile, D.; Khanna, R.; Auroy, P. *Langmuir* **1999**, *15*, 2551.

(11) Strobl, G. *The Physics of Polymers*, 2nd ed.; Springer-Verlag: Berlin and Heidelberg, Germany, 1996 and 1997.

(12) Tsui, O. K. C.; Wang, X. P.; Ho, Jacob, Y. L.; Ng, T. K.; Xiao, Xudong *Macromolecules* **2000**, *33*, 4198.

(13) Williams, M. L.; Landel, R. F.; Ferry, J. D. *J. Am. Chem. Soc.* **1955**, *77*, 3701.

(14) Vogel, H. *Physik, Z.* **1921**, *22*, 645. Tammann, G.; Hesse, W. *Z. Anorg. Allgem. Chem.* **1926**, *156*, 245.

(15) Angell, C. A. *J. Non-Cryst. Solids* **1991**, *131−133*, 13. Angell, C. A. *Science* **1995**, *67*, 1924.

(16) Adam, G.; Gibbs, J. H. *J. Chem. Phys.* **1965**, *43*, 139.

(17) Kauzmann, W. *Chem. Rev.* **1948**, *43*, 219.

(18) Greenwood, J. A.; Johnson, K. L. *Philos. Mag. A* **1981**, *43*, 697.

(19) Johnson, K. L.; Kendall, K.; Roberts, A. D. *J. Am. Chem. Soc.* **1971**, *93*, 301.

(20) Zhao, W.; Zhao, X.; Rafailovich, M. H.; Sokolov, J.; Composto, R. J.; Smith, S. D.; Satkowski, M.; Russell, T. P.; Dozier, W. D.; Mansfield, T. *Macromolecules* **1993**, *26*, 561.

(21) Paiva, A.; Sheller, N.; Foster, M. D.; Crosby, A. J.; Shull, K. R. *Macromolecules* **2000**, *33*, 1878.

(22) We note that the onset frequency of the plateau region shown in Figure 6 of ref 12 for a 150 nm thick P*t*BuA film is ~100 Hz at 55 °C. However, as shown in Figure 3 of this paper, the onset frequency of the 130 nm thick sample is only ~20 Hz at the same temperature. Simply from the thin film thickness dependence of the onset frequency, one will expect a thinner film to have a higher onset frequency. Result of this comparison suggests that the AFM cantilevers used in the present experiment are stiffer than those used in ref 12 although both have the same nominal force constant.

(23) Foster, M. D. Private discussion.

(24) DeMaggio, G. B.; Frieze, W. E.; Gidley, D. W.; Zhu, M.; Hristov, H. A.; Yee, A. F. *Phys. Rev. Lett.* **1997**, *78*, 1524.

(25) Blum, F. D.; Xu, G.; Liang, M.; Wade, C. *Macromolecules* **1996**, *29*, 874.

MA0018953